View metadata, citation and similar papers at core.ac.uk

brought to you by CORE

provided by Elsevier - Publisher Connector

Current Biology 23, 731–736, April 22, 2013 ©2013 Elsevier Ltd All rights reserved http://dx.doi.org/10.1016/j.cub.2013.03.039

Report

NMII Forms a Contractile Transcellular Sarcomeric Network to Regulate Apical Cell Junctions and Tissue Geometry

Seham Ebrahim,[1,6] Tomoki Fujita,[2,6] Bryan A. Millis,[1] Elliott Kozin,[1] Xuefei Ma,[3] Sachiyo Kawamoto,[3] Michelle A. Baird,[4] Michael Davidson,[4] Shigenobu Yonemura,[5] Yasuo Hisa,[2] Mary Anne Conti,[3] Robert S. Adelstein,[3] Hirofumi Sakaguchi,[2,*] and Bechara Kachar[1,*]

[1]Laboratory of Cell Structure and Dynamics, National Institute on Deafness and Other Communication Disorders, National Institutes of Health, Bethesda, MD 20892, USA

[2]Department of Otolaryngology-Head and Neck Surgery, Kyoto Prefectural University of Medicine, Kyoto 602-8566, Japan

[3]Laboratory of Molecular Cardiology, National Heart, Lung, and Blood Institute, National Institutes of Health, Bethesda, MD 20814, USA

[4]National High Magnetic Field Laboratory, Florida State University, Tallahassee, FL 32310, USA

[5]Electron Microscope Laboratory, RIKEN Center for Developmental Biology, Kobe 650-0047, Japan

Summary

Nonmuscle myosin II (NMII) is thought to be the master integrator of force within epithelial apical junctions, mediating epithelial tissue morphogenesis and tensional homeostasis [1–3]. Mutations in NMII are associated with a number of diseases due to failures in cell-cell adhesion [4–8]. However, the organization and the precise mechanism by which NMII generates and responds to tension along the intercellular junctional line are still not known. We discovered that periodic assemblies of bipolar NMII filaments interlace with perijunctional actin and α-actinin to form a continuous belt of muscle-like sarcomeric units (~400–600 nm) around each epithelial cell. Remarkably, the sarcomeres of adjacent cells are precisely paired across the junctional line, forming an integrated, transcellular contractile network. The contraction/relaxation of paired sarcomeres concomitantly impacts changes in apical cell shape and tissue geometry. We show differential distribution of NMII isoforms across heterotypic junctions and evidence for compensation between isoforms. Our results provide a model for how NMII force generation is effected along the junctional perimeter of each cell and communicated across neighboring cells in the epithelial organization. The sarcomeric network also provides a well-defined target to investigate the multiple roles of NMII in junctional homeostasis as well as in development and disease.

Results and Discussion

We examine the organization of NMII in the apical junctional complex (AJC) using the organ of Corti, which is an epithelial sheet formed by a checkerboard mosaic of sensory (hair cells, HCs) and nonsensory epithelial cells, flanked medially by a purely nonsensory epithelium of hexagonally packed inner sulcus cells (ISCs). We initially sought to investigate the extent that NMII is involved in regulating the apical perimeter and surface area of the various cell types. To this end, we conducted a chemical inhibition experiment using the NMII-specific inhibitor blebbistatin [9] in explant cultures of the organ of Corti dissected from P2 mice. Following blebbistatin exposure, the apical surfaces of cells exhibited striking modifications in their perimeter and area when compared with the control (Figure 1A). These effects were reversed after the washout of blebbistatin. A morphometric analysis of the cellular effects of blebbistatin showed a significant ($p < 0.01$) increase (3%–30%) in perimeter or junctional length (see Figure S1A available online), and a corresponding significant ($p < 0.01$) increase in apical cell-surface area (Figure S1B). Upon addition of blebbistatin, the perimeter of HCs also deviated from circularity, as verified by changes in the calculated roundness factor (RF, Figure S1C). This loss of circularity combined with increase of surface area is consistent with overall tension reduction at the cell perimeter on addition of blebbistatin, indicating that the circumferential junctional actomyosin belt is maintained under tension by NMII. On a global level, blebbistatin caused a reversible expansion of the organ of Corti, which was greater along the radial direction as compared with the longitudinal direction (R/L, Figure S1D). Taken together, these results highlight the dependence of junctional length and apical surface area, as well as concerted changes in the geometry of the epithelium, on NMII function.

Because our data support a role for NMII in modulating epithelial apical perimeter we sought to assess the precise localization of NMII isoforms along the AJC. Immunofluorescence of NMIIC and NMIIB showed a remarkable pattern of distribution as regularly spaced puncta along the perimeter of each cell. This pattern is clearly observed in both ISCs (Figure 1B) and in HCs (Figures S1E and S1F). Conversely, immunoreactivity for NMIIA, a major NMII isoform at stress fibers and circumferential actin bundles in spreading cells [10, 11], was barely detectable around the apical perimeter of these cells (Figure S1G). Measuring the relative fluorescence intensity of actin and NMIIB or NMIIC along the junctional line, we observed an inversely correlated periodic modulation, with low actin density at the center of the NMII fluorescence puncta and higher actin density in spaces between them (Figure 1B, inset), resembling the striated pattern of myosin and actin in muscle sarcomeres. Strikingly, fluorescence NMII puncta from adjacent cells consistently paired in register across the junctional line, appearing collectively as a transcellular network across the epithelial sheet (Figures 1C and 1D). At tricellular contacts of ISCs, the NMII fluorescence puncta localized precisely at the corner of each cell in a regular triangular arrangement (Figure 1C, arrows, and Figure 1D). The relative fluorescence intensity of NMIIC puncta was higher at tricellular junctions (5.07 ± 0.9, $n = 50$) than along bicellular junctions (3.2 ± 0.8, $n = 50$). Because tricellular junctions experience additional tensions [12], this observation raises the possibility that NMII could be

[6]These authors contributed equally to this work

*Correspondence: hiro-s@koto.kpu-m.ac.jp (H.S.), kacharb@nidcd.nih.gov (B.K.)

CrossMark

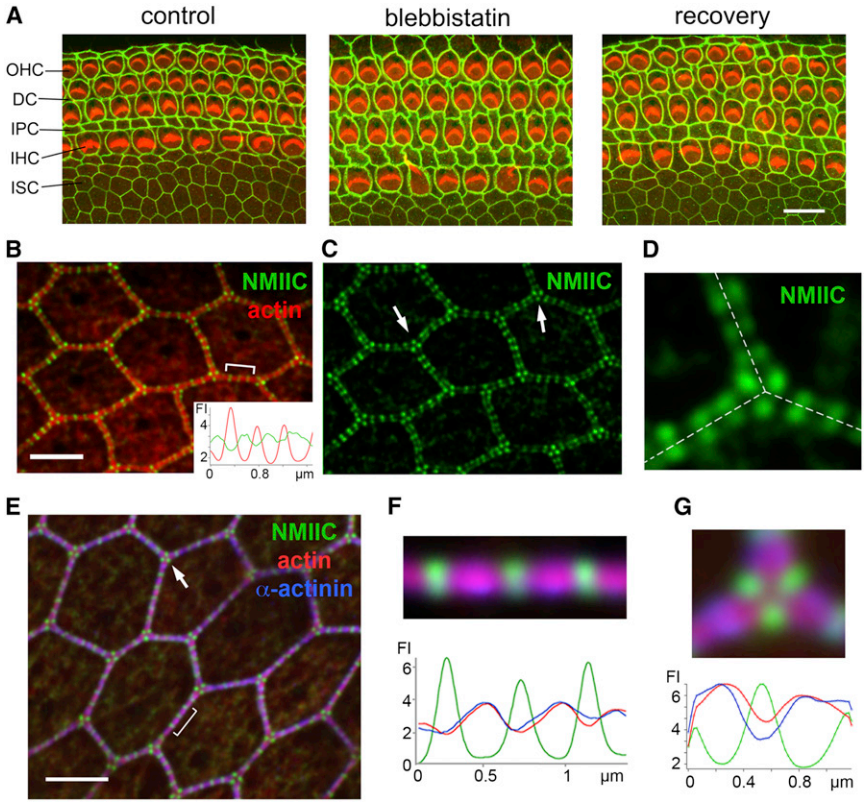

Figure 1. NMII Regulates Apical Epithelial Geometry and Alternates with Actin and α-Actinin1 along the Apical Junctional Line

(A) Apical surface of mouse organ of Corti explant cultures with ZO1 (green) and actin (red) labeling, showing changes in apical geometry of the epithelia at the cell and tissue level before (control) and after (blebbistatin) treatment with blebbistatin and after blebbistatin was washed out (recovery). OHC, outer hair cells; DC, Deiters' cells; IPC, inner pillar cells; IHC, inner hair cells; ISC, inner sulcus cells.

(B and C) Localization of NMIIC (green) in periodic puncta along cell-cell contacts of rat ISCs, with actin in red. Inset, tracking of red and green fluorescence intensity (FI) along bracketed region in (B). Arrows in (C) show triangular arrangement of NMIIC puncta at tricellular contacts.

(D) NMIIC fluorescence puncta in adjacent cells align precisely across the junctional line (dashed line).

(E) NMIIC (green) and α-actinin1 (blue) immunofluorescence in ISCs, with actin in red. Arrows highlight triangular arrangement of NMIIC puncta at tricellular contacts (arrow).

(F) Magnification of bracket in (E): actin and α-actinin1 colocalize and alternate with regions of high NMIIC intensity. Below: corresponding fluorescence intensity (FI) profile of NMIIC (green), actin (red), and α-actinin1 (blue).

(G) Magnification of tricellular junction from (E), showing alternation of NMIIC (green) with actin (red) and α-actinin1 (blue). Below: corresponding FI profile of NMIIC (green), actin (red), and α-actinin1 (blue).

Scale bars represent 10 μm in (A) and 3 μm in (B)–(E). See also Figure S1.

distributed in a tension-dependent manner [13] as part of a self-regulated tensional homeostasis.

The resemblance of the NMII/actin alternation to that in muscle sarcomeres prompted us to test for the presence and distribution of α-actinin, a member of the spectrin family that crosslinks antiparallel actin filaments in the Z line of muscle [14]. Immunofluorescence revealed that nonmuscle α-actinin1 is present along the junctional line in a periodic pattern alternating with NMII puncta in both ISCs (Figure 1E) and HCs (Figure S1H). Fluorescence intensity analysis along the junctional line confirmed the precise alternation of NMII puncta with regions of high α-actinin1 density, and also the coincidence of α-actinin1 and actin (Figures 1F, 1G, and S1I). The average distance between consecutive NMII puncta in HCs was 436 ± 93 nm (median = 479 nm, n = 101), and in ISCs it was 452 ± 65 nm (median = 449 nm, n = 101). The close-up view in Figure 1G shows the alternation of NMII and actin/α-actinin1 around the corners of a tricellular junction. Further confirmation of the periodic pattern of localization of NMII at the AJC was obtained by exogenously expressing NMIIC-GFP in organ of Corti explants (Figure S1J).

We tested for orientation of the NMII bipolar filaments along the junctional line by expressing a double-tagged NMIIC (with the fluorescence probe mEmerald at the N-terminal myosin head and the fluorescence probe mCherry at the C-terminal myosin tail) in cultured organ of Corti. Each tail-specific mCherry fluorescence punctum of the double-tagged NMIIC appeared as a central red spot flanked on both sides along the junctional line by green mEmerald head-specific fluorescence puncta (Figures 2A and 2B). The orientation of the bipolar filaments parallel to the junctional line was confirmed using tissue from a transgenic mouse expressing a GFP-tag at the C-terminal tail of NMIIC that was coimmunolabeled with an NMIIC N terminus-specific antibody (Figure 2C). To assess the length of each array of bipolar NMII filaments, we measured the distance between the head-head maxima. The measured length (402 nm ± 53 nm, n = 10) was at the upper end of the reported length distribution range (~280–400 nm) of NMII bipolar filaments in nonmuscle cells [15–17] and significantly smaller than muscle myosin II bipolar filaments, which range from ~2 μm in vertebrates [18] to ~10 μm in invertebrates [19]. Although the lengths of the bipolar NMII filaments in the AJC were relatively consistent, some degree of variation was observed in the separation between bipolar filaments (Figures 2A-2C). These results are consistent with an arrangement of NMII bipolar filaments within small regular sarcomeric units, where the tail regions of NMII are the center points of each sarcomere, assembled in series to form a belt along the junctional line of each cell, as illustrated in the model in Figure 2D. The variation in sarcomere lengths observed is likely due to stochastic fluctuations in sarcomere contraction/relaxation [20] or intrinsic variations in the length of actin and extent of actin crosslinking by α-actinin [21].

Labeling the head and tail of NMII additionally provided a clearer view of the registry between sarcomeres of adjacent cells across the junctional line (Figure 2C, illustrated in Figure 2D). NMII puncta at tricellular junctions were also arranged in a bipolar configuration but formed an angle with the midpoint tail fluorescence label consistently pointing to the tricellular corner (Figure 2C, arrows). This suggests that the midpoint (tail-rich region) of each sarcomere is physically

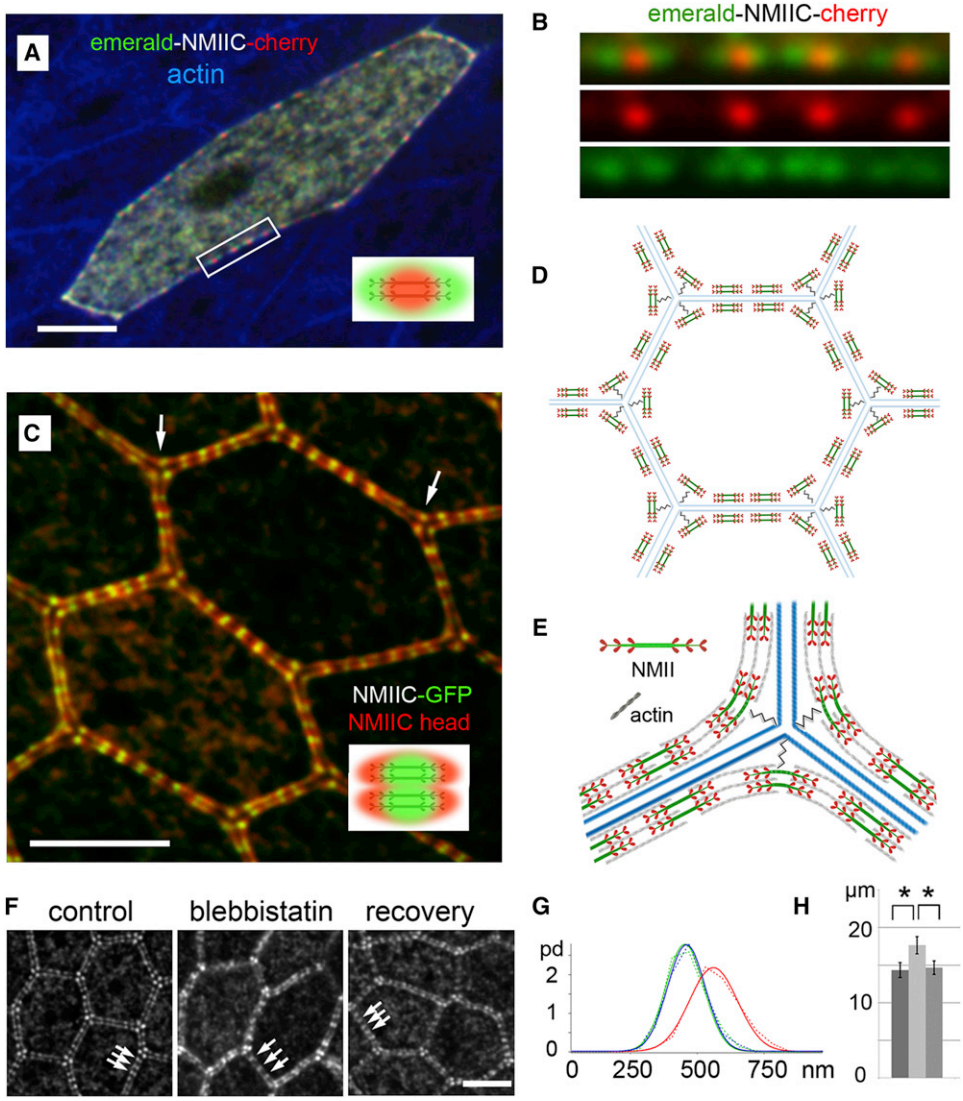

Figure 2. Sarcomeric Organization and Orientation of Bipolar NMIIC Filaments along the Epithelial AJC

(A) Nonsensory epithelial cell in rat organ of Corti expressing double-tagged NMIIC (N terminus, mEmerald/green; C terminus mCherry/red), with actin in blue. Inset shows a diagram of diffraction-limited appearance of double-labeled NMII filaments.

(B) Close-up of four bipolar NMIIC filaments from box in (A).

(C) Bipolar NMIIC filaments align end-to-end along the junctional line between ISCs from a NMIIC-GFP mouse, with GFP-tag at NMIIC-tail (green) and anti-NMIIC-head antibody (red). Arrows point to bipolar arrangement of NMII at tricellular junctions. Inset shows a diagram of the diffraction-limited image of double-labeled NMII filaments.

(D) Illustration of the relationship of the sarcomeric belt of an epithelial cell and that of six neighboring cells, showing the paring of individual NMII sarcomeres across the junctional line.

(E) Model of the arrangement of bipolar NMIIC filaments at a tricellular junction. The "spring-like" symbol represents the putative tether between NMII and the corner of the cell at tricellular contacts.

(F) NMIIC sarcomere length along apical junctions of ISCs in rat organ of Corti cultures before (control) and after (blebbistatin) treatment with blebbistatin and after washout of blebbistatin (recovery).

(G) Probability distribution (pd) of sarcomere length in ISCs of control (green), blebbistatin (red), and recovery (blue). Dashed lines, measured data; solid lines, Gaussian fits. Calculated Gaussian widths are: control = 198.4 ± 3.7 nm, blebbistatin-treated = 253 ± 8.9 nm, and recovery = 200 ± 9.3 nm.

(H) ISC apical junctional perimeter in control (dark gray), blebbistatin (light gray), and recovery (medium gray) explants. Data represent means ± SD. Asterisk represents significant to $p < 0.01$.

Scale bars represent 3 μm. See also Figure S2.

tethered to the tricellular contacts, pinning the tensed sarcomeric belt to the corners of the cell, whereas the head regions stay bound to actin filaments, causing the bending of the NMII sarcomeric units, as illustrated in Figure 2E.

To test for contractility of the NMII sarcomeres, we repeated the blebbistatin inhibition experiment in rat organ of Corti cultures and measured changes in the distance between consecutive NMII immunofluorescence puncta as an indicator of changes in sarcomere length, as well as changes in junctional length or cell perimeter. Comparing the sarcomere length before and after 1 hr of 50 μM blebbistatin inhibition, we observed that the average sarcomere length in control

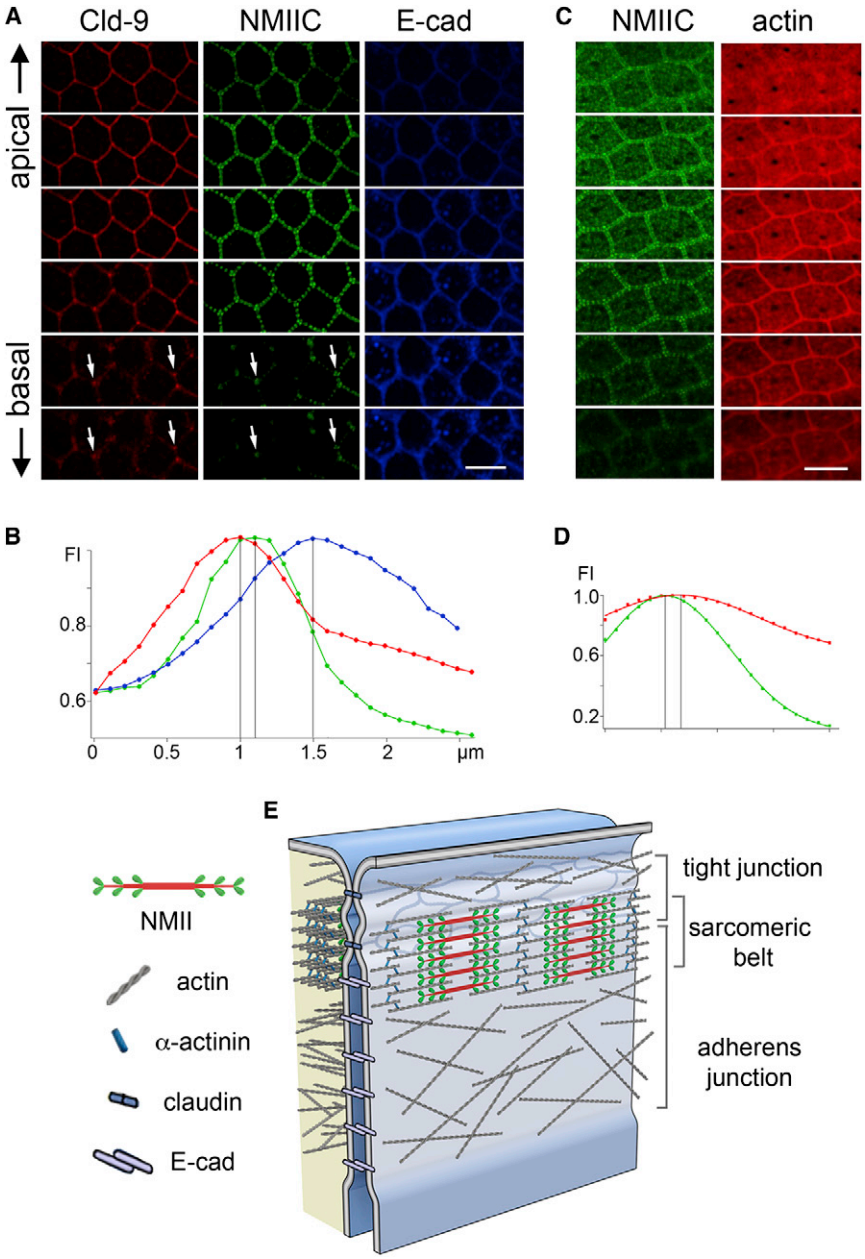

Figure 3. Localization of the Sarcomeric Belt Relative to the Tight and Adherens Junctions of the AJC

(A) ISCs of the organ of Corti from a P2 NMIIC-GFP mouse showing localization of NMIIC-GFP (green) relative to the tight junction protein claudin 9 (red, Cld-9) and adherens junction protein E-cadherin (blue, E-cad) along the z axis. Optical sectioning (200 nm/step) is shown top to bottom from apical toward the basal surface.

(B) Fluorescence intensity (FI) plots of NMIIC (green), claudin 9 (red), and E-cadherin (blue) along the z axis.

(C) ISCs from a NMIIC-GFP mouse costained for actin (red). Optical sectioning (200 nm/step) toward the basal surface reveals the characteristic NMIIC-GFP fluorescence signal (green), which peaks at the upper portion of the actin staining.

(D) Fluorescence intensity (FI) of NMIIC (green) and actin (red) along the z axis.

(E) Diagram illustrating the location of the NMII sarcomeric belt at the interface of the tight (claudin 9) and adherens (E-cadherin) junction components of the AJC.

Scale bars represent 4 μm. See also Figure S3.

ISCs (461 ± 70 nm, n = 418) increased significantly ($p < 0.001$), by ~24%, with blebbistatin treatment (570 ± 97 nm, n = 418) and was restored (463 ± 72 nm, n = 418) after its washout (Figures 2F and 2G). Similarly, sarcomere length in HCs (424 ± 103 nm, n = 467) increased significantly, by ~20% ($p < 0.001$), after blebbistatin treatment (516 ± 136 nm, n = 669) and was reversed (460 ± 90 nm, n = 464) after its washout (Figures S2A and S2B). The blebbistatin-induced changes in sarcomere length matched the changes in junctional length. The average junctional length for ISCs (14.3 ± 1 μm, n = 100) increased significantly, by ~23% ($p < 0.01$), after blebbistatin inhibition (17.6 ± 1.1 μm, n = 100) and was restored (14.6 ± 0.9 μm, n = 100) after blebbistatin was washed out (Figure 2H). The average junctional length for HCs (21.3 ± 1 μm, n = 100) increased by ~10% ($p < 0.01$) after blebbistatin inhibition (23 ± 1.1 μm, n = 100) and was restored (21.4 ± 1.2 μm, n = 100) after it was washed out (Figure S2C). These results are consistent with a sarcomere-based "purse-string" model [22, 23] for cortical tensional homeostasis. The registry between sarcomeres across the junctional line was maintained regardless of contractile state (Figure 2F, arrows), providing further evidence for the existence of some form of mechanical coupling or tight functional coordination [24] of sarcomeres across the junctional line. This is likely an important component of a physical network, along which the force balance interplay between tensions generated at the AJC and cytoskeleton of a single cell is transmitted across the epithelia as a whole.

To examine the precise location of the NMII sarcomeric belt in relation to the stratified two-layer (tight and adherens junction) organization of the AJC, we acquired z stacks of confocal images at 50 nm intervals of the apical junctional region of organ of Corti tissue from NMIIC-GFP mice, costained for tight and adherens junction-specific proteins, claudin 9 and E-cadherin, respectively. Figure 3A shows a series of images from this set at 200 nm intervals. The immunofluorescence signal of claudin 9 along the z axis peaked at the apical-most region of the AJC, and that of E-cadherin was at the basal-most side. The fluorescence intensity of NMIIC-GFP overlapped partially with both claudin 9 and E-cadherin immunofluorescence (Figure 3A). Of note, the apical-basal distribution of NMIIC and claudin 9 persisted together at tricellular junctions (Figure 3A, arrows), deeper in the basal direction than immunofluorescence at bicellular junctions. This observation, combined with the knowledge that the network of tight junctions extends basolaterally when converging at tricellular contacts [25, 26], suggests an interaction between the tail domain of NMII and tricellular tight junction components (Figure 2E).

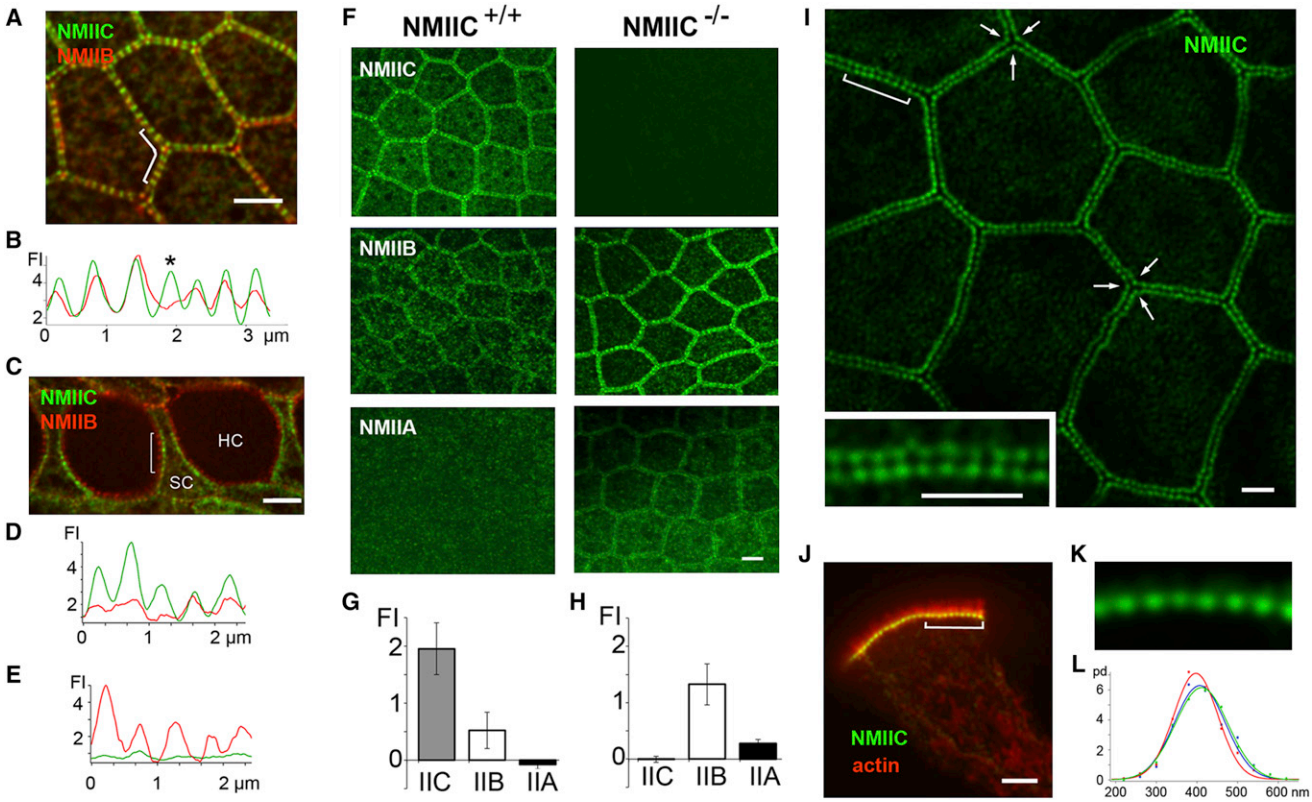

Figure 4. Differential Distribution of NMII Isoforms and Evidence for Compensation in Absence of NMIIC

(A) Apical surface of ISCs from a P2 NMIIC-GFP mouse immunolabeled with anti-NMIIB antibody. Both NMIIB (red) and NMIIC (green) colocalize and distribute symmetrically across homomeric junctions between ISCs.

(B) Fluorescence intensity (FI) along bracketed area in (A); NMIIB/NMIIC ratio varies across NMII puncta (asterisk).

(C) The distribution of the NMIIB (red) and NMIIC (green) is asymmetric across heteromeric hair cell (HC)/supporting cell (SC) junctions.

(D and E) Plots of the fluorescence intensity along the HC and SC perimeters within the bracketed region in (C).

(F) ISCs from P6 NMIIC+/+ and NMIIC−/− mice stained with NMIIC-, NMIIB-, and NMIIA-specific antibodies (green).

(G and H) Quantification of NMIIA, NMIIB, and NMIIC immunofluorescence intensity at cell-cell contacts in NMIIC+/+ (G) and NMIIC−/− (H). Data are represented as mean fluorescence intensity ± SD.

(I) Apical surface of epithelium from the small intestine of a P2 NMIIC-GFP mouse showing the periodic distribution of NMIIC-GFP along the apical perimeter of enterocytes. Arrows highlight the precise triangular arrangement at tricellular junctions. Inset is a close-up view of the bracketed region, showing that puncta from adjacent cells line up in register across the junctional line.

(J) A side view of an isolated enterocyte, showing the characteristic actin-based (red) microvilli projecting from the apical surface with the periodic NMIIC (green) puncta along the apical junctional region.

(K) Close-up view of the periodic NMIIC puncta from the bracketed region in (J).

(L) Probability distribution (pd) of NMIIC sarcomere length in small intestine (red), large intestine (blue), and stomach (green).

Scale bars represent 2.5 μm. See also Figure S4.

To estimate the relative localization of each tagged protein along the z axis, we plotted the immunofluorescence intensity values after correcting for axial (z axis) chromatic aberration (Figure S3) and determined the points of fluorescence maxima. We found that the NMIIC-GFP fluorescence maxima were ~108 ± 27 nm (n = 13) below the claudin 9 fluorescence maxima and ~350 ± 86 nm (n = 13) above the maxima for the E-cadherin (Figure 3B). These results are consistent with the localization of the NMIIC sarcomeres at a midpoint of the AJC, likely forming a distinct structure that overlaps partially with both the tight junction and the adherens junction. We also assessed the localization of NMIIC relative to the total circumferential actin belt by labeling organ of Corti tissue from a P2 rat with NMIIC and Alexa Fluor 568-conjugated phalloidin. The z stack of confocal images obtained (a substack of which is shown in Figure 3C) showed that the NMIIC fluorescence distribution does not encompass all the junctional actin but is consistent with an association with a subset of the circumferential actin belt (Figure 3D). A model proposing the localization of the NMII sarcomeric belt within the AJC at the interface of tight and adherens junctions is presented in Figure 3E.

Double-labeling experiments showed colocalization of NMIIB and NMIIC along homomeric junctions (e.g., between ISCs in Figure 4A), suggesting some degree of functional redundancy. Conversely, NMIIB and NMIIC sarcomeres consistently distributed asymmetrically across the junctional line of heteromeric junctions (e.g., between HCs and SCs in Figure 4C). Because of their differential kinetic properties [27], the asymmetric distribution of NMII isoforms may contribute to the generation of distinct spatiotemporal distributions of forces across the junctional line and help in sculpting different cell morphologies within the epithelia.

It is known that mutations in individual NMII isoforms are linked to the onset and progression of a number of human diseases [4, 5], including hearing loss [4, 6, 7]. To our knowledge, compensation between NMII isoforms has not been reported,

and NMIIA and NMIIB knockout mice are both embryonic lethal. However, NMIIC−/− mice develop normally to at least three months of age [28], and the immunofluorescence of NMIIA and NMIIB in the AJC was significantly increased in these mice compared to wild-type (Figures 4F–4H), suggesting potential compensatory effects between NMII isoforms.

To determine whether the sarcomeric organization of NMII is present in other epithelial tissues, we examined the pattern of distribution of NMIIC in intestinal enterocytes (Figures 4I–4K) and stomach epithelial cells (data not shown) of the NMIIC-GFP mouse. The average distance between NMII puncta was 398 ± 58 nm (n = 542) in small intestine, 410 ± 66 nm (n = 539) in large intestine, and 414 ± 64 nm (n = 488) in stomach epithelial cells (Figure 4L), indicating a consistent ~400–500 nm range across various epithelial tissues.

In this study, we uncover the likely ubiquitous sarcomeric organization of NMII within the epithelial AJC. The localization of the sarcomeric belt at the interface of the tight and adherens junctions provides a well-defined target to investigate the multiple roles of NMII in tensional homeostasis. Knowledge pertaining to the differential localization of NMII isoforms can also be used to explore differences in biomechanical properties in the AJC of various tissues during development and disease, making our findings relevant across biomedical disciplines.

Supplemental Information

Supplemental Information includes four figures and Supplemental Experimental Procedures and can be found with this article online at http://dx.doi.org/10.1016/j.cub.2013.03.039.

Acknowledgments

We thank Juan Pablo Inda, Agnieszka Rzadzinska, Felipe Salles, Alex Rivero, Jian Mao, and Yuhai Dai for their participation in early experiments and Ethan Tyler for the artwork. This work was supported by the Intramural Programs of the National Institute on Deafness and Other Communication Disorders and the National Heart, Lung, and Blood Institute, National Institutes of Health, and by Ministry of Education, Culture, Sports, Science and Technology/Japan Society for the Promotion of Science KAKENHI Grant number 23592491. All rodent procedures were carried out in accordance with NIDCD and NHLBI Animal Care and Use Committee guidelines.

Received: February 4, 2013
Revised: March 12, 2013
Accepted: March 14, 2013
Published: April 4, 2013

References

1. Bertet, C., Sulak, L., and Lecuit, T. (2004). Myosin-dependent junction remodelling controls planar cell intercalation and axis elongation. Nature *429*, 667–671.
2. Conti, M.A., Even-Ram, S., Liu, C., Yamada, K.M., and Adelstein, R.S. (2004). Defects in cell adhesion and the visceral endoderm following ablation of nonmuscle myosin heavy chain II-A in mice. J. Biol. Chem. *279*, 41263–41266.
3. Yamamoto, N., Okano, T., Ma, X., Adelstein, R.S., and Kelley, M.W. (2009). Myosin II regulates extension, growth and patterning in the mammalian cochlear duct. Development *136*, 1977–1986.
4. Zhang, Y., Conti, M.A., Malide, D., Dong, F., Wang, A., Shmist, Y.A., Liu, C., Zerfas, P., Daniels, M.P., Chan, C.-C., et al. (2012). Mouse models of MYH9-related disease: mutations in nonmuscle myosin II-A. Blood *119*, 238–250.
5. Heissler, S.M., and Manstein, D.J. (2013). Nonmuscle myosin-2: mix and match. Cell. Mol. Life Sci. *70*, 1–21.
6. Lalwani, A.K., Goldstein, J.A., Kelley, M.J., Luxford, W., Castelein, C.M., and Mhatre, A.N. (2000). Human nonsyndromic hereditary deafness DFNA17 is due to a mutation in nonmuscle myosin MYH9. Am. J. Hum. Genet. *67*, 1121–1128.
7. Seri, M., Cusano, R., Gangarossa, S., Caridi, G., Bordo, D., Lo Nigro, C., Ghiggeri, G.M., Ravazzolo, R., Savino, M., Del Vecchio, M., et al. (2000). Mutations in MYH9 result in the May-Hegglin anomaly, and Fechtner and Sebastian syndromes. The May-Hegglin/Fechtner Syndrome Consortium. Nat. Genet. *26*, 103–105.
8. Xia, Z.K., Yuan, Y.C., Yin, N., Yin, B.L., Tan, Z.P., and Hu, Y.R. (2012). Nonmuscle myosin IIA is associated with poor prognosis of esophageal squamous cancer. Dis. Esophagus *25*, 427–436.
9. Straight, A.F., Cheung, A., Limouze, J., Chen, I., Westwood, N.J., Sellers, J.R., and Mitchison, T.J. (2003). Dissecting temporal and spatial control of cytokinesis with a myosin II Inhibitor. Science *299*, 1743–1747.
10. Cai, Y., Biais, N., Giannone, G., Tanase, M., Jiang, G., Hofman, J.M., Wiggins, C.H., Silberzan, P., Buguin, A., Ladoux, B., and Sheetz, M.P. (2006). Nonmuscle myosin IIA-dependent force inhibits cell spreading and drives F-actin flow. Biophys. J. *91*, 3907–3920.
11. Burnette, D.T., Manley, S., Sengupta, P., Sougrat, R., Davidson, M.W., Kachar, B., and Lippincott-Schwartz, J. (2011). A role for actin arcs in the leading-edge advance of migrating cells. Nat. Cell Biol. *13*, 371–381.
12. Trichas, G., Smith, A.M., White, N., Wilkins, V., Watanabe, T., Moore, A., Joyce, B., Sugnaseelan, J., Rodriguez, T.A., Kay, D., et al. (2012). Multi-cellular rosettes in the mouse visceral endoderm facilitate the ordered migration of anterior visceral endoderm cells. PLoS Biol. *10*, e1001256.
13. Fernandez-Gonzalez, R., Simoes, Sde.M., Röper, J.-C., Eaton, S., and Zallen, J.A. (2009). Myosin II dynamics are regulated by tension in intercalating cells. Dev. Cell *17*, 736–743.
14. Squire, J.M. (1997). Architecture and function in the muscle sarcomere. Curr. Opin. Struct. Biol. *7*, 247–257.
15. Niederman, R., and Pollard, T.D. (1975). Human platelet myosin. II. In vitro assembly and structure of myosin filaments. J. Cell Biol. *67*, 72–92.
16. Svitkina, T.M., Surguchova, I.G., Verkhovsky, A.B., Gelfand, V.I., Moeremans, M., and De Mey, J. (1989). Direct visualization of bipolar myosin filaments in stress fibers of cultured fibroblasts. Cell Motil. Cytoskeleton *12*, 150–156.
17. Verkhovsky, A.B., Svitkina, T.M., and Borisy, G.G. (1995). Myosin II filament assemblies in the active lamella of fibroblasts: their morphogenesis and role in the formation of actin filament bundles. J. Cell Biol. *131*, 989–1002.
18. Gordon, A.M., Huxley, A.F., and Julian, F.J. (1966). The variation in isometric tension with sarcomere length in vertebrate muscle fibres. J. Physiol. *184*, 170–192.
19. Sellers, J.R., and Kachar, B. (1990). Polarity and velocity of sliding filaments: control of direction by actin and of speed by myosin. Science *249*, 406–408.
20. Russell, R.J., Grubbs, A.Y., Mangroo, S.P., Nakasone, S.E., Dickinson, R.B., and Lele, T.P. (2011). Sarcomere length fluctuations and flow in capillary endothelial cells. Cytoskeleton (Hoboken) *68*, 150–156.
21. Littlefield, R.S., and Fowler, V.M. (2008). Thin filament length regulation in striated muscle sarcomeres: pointed-end dynamics go beyond a nebulin ruler. Semin. Cell Dev. Biol. *19*, 511–519.
22. Baker, P.C., and Schroeder, T.E. (1967). Cytoplasmic filaments and morphogenetic movement in the amphibian neural tube. Dev. Biol. *15*, 432–450.
23. Hildebrand, J.D. (2005). Shroom regulates epithelial cell shape via the apical positioning of an actomyosin network. J. Cell Sci. *118*, 5191–5203.
24. Pellegrin, S., and Mellor, H. (2007). Actin stress fibres. J. Cell Sci. *120*, 3491–3499.
25. Ikenouchi, J., Furuse, M., Furuse, K., Sasaki, H., Tsukita, S., and Tsukita, S. (2005). Tricellulin constitutes a novel barrier at tricellular contacts of epithelial cells. J. Cell Biol. *171*, 939–945.
26. Masuda, S., Oda, Y., Sasaki, H., Ikenouchi, J., Higashi, T., Akashi, M., Nishi, E., and Furuse, M. (2011). LSR defines cell corners for tricellular tight junction formation in epithelial cells. J. Cell Sci. *124*, 548–555.
27. Wang, A., Ma, X., Conti, M.A., and Adelstein, R.S. (2011). Distinct and redundant roles of the non-muscle myosin II isoforms and functional domains. Biochem. Soc. Trans. *39*, 1131–1135.
28. Ma, X., Jana, S.S., Conti, M.A., Kawamoto, S., Claycomb, W.C., and Adelstein, R.S. (2010). Ablation of nonmuscle myosin II-B and II-C reveals a role for nonmuscle myosin II in cardiac myocyte karyokinesis. Mol. Biol. Cell. *21*, 3952–3962.